Materials Science-Poland
Volume 42 Issue 3 · pp. 100–110 · DOI: 10.2478/msp-2024-0035

Materials Science-Poland

Copper oxide–ferric oxide nanocomposite: Synthesis, characterization, and antibacterial and antifungal properties

Research Article

Mohamed Elnouby[1], Marwa Nabil[2], Abdulaziz A. Al-Askar[3], Przemysław Kowalczewski[4], Said Behiry[5], Ahmed Abdelkhalek[6]*

[1] *Advanced Technology and New Materials Research Institute, City for Scientific Research and Technology Applications, New Borg El-Arab City, Alexandria, Egypt*
[2] *Electronic Materials Researches Department, Advanced Technology and New Materials Research Institute, City for Scientific Research and Technology Applications, New Borg El-Arab City, Alexandria, Egypt*
[3] *Department of Botany and Microbiology, College of Science, King Saud University, Riyadh, Saudi Arabia*
[4] *Department of Food Technology of Plant Origin, Poznań University of Life Sciences, Poznań, Poland*
[5] *Agricultural Botany Department, Faculty of Agriculture (Saba Basha), Alexandria University, Alexandria, Egypt*
[6] *City of Scientific Research and Technological Applications, New Borg El-Arab City, Alexandria, Egypt*

Received 12 June 2024; Accepted 19 September 2024

Abstract: Recently, copper oxide–ferric oxide nanocomposites (CuO/Fe_2O_3-NCs) have gained popularity and are widely employed in various applications. However, their effectiveness against phytopathogens has not been studied yet. This study investigates the synthesis and characterization of CuO/Fe_2O_3-NCs using the hydrothermal technique. X-ray diffraction (XRD), transmission electron microscopy (TEM), energy-dispersive X-ray spectroscopy (EDX), and Fourier-transform infrared spectroscopy (FTIR) were used to characterize the produced nanocomposite (NC). EDX and TEM analyses revealed the presence of Cu, Fe, and O elements. The NC had a polygonal shape with sides around 12 nm, spherical CuO particles of 7–10 nm, and plate-like Fe_2O_3. XRD measurements confirmed the crystal and hexagonal structures of CuO and Fe_2O_3. The XRD patterns of CuO/Fe_2O_3 showed the characteristic peaks of (−111) and (004) reflections for CuO at 35.69° and 37.73°. The FTIR spectra showed characteristic lines at 525 and 567 cm^{-1} for the Cu–O bond and Fe–O stretching modes of Fe_2O_3, respectively. The antifungal activity of CuO/Fe_2O_3-NCs showed significant growth inhibition of *Fusarium oxysporum*, *Rhizoctonia solani*, and *Botrytis cinerea* by up to 71, 50, and 81%, respectively, at 100 µg/mL. At 50 µg/mL, the antibacterial test revealed inhibition zones of 12.33 mm for *Pectobacterium carotovorum*, 9.33 mm for *Streptomyces scabies*, 10.67 mm for *Pectobacterium atrosepticum*, and 14.67 mm for *Ralstonia solanacearum*. The results show that CuO/Fe_2O_3-NCs can efficiently suppress the growth of various fungal and bacterial strains, making them potential antimicrobial agents against phytopathogenic microorganisms.

Keywords: *Copper oxide–ferric oxide • Nanocomposite • TEM • FTIR • Antibacterial • Antifungal*

1. Introduction

Nanotechnology is a field of materials science that deals with manipulating fine-sized matter within a range of 1–100 nm. These nanomaterials, due to their large surface area-to-volume ratio, have unique physiochemical, magnetic, optical, and electrical properties [1]. Iron oxide-based nanoparticles are a part of these well-known transition metal oxides. They have been prepared using various preparation methods, including wet chemical methods [2], liquid phase deposition [3], and green preparation methods [4]. Transition metal oxide nanoparticles have been characterized by unique properties [5]. Particularly, iron oxide nanomaterials have been used and studied for various applications, such as water treatment [6], drug delivery [7], catalysis [8], water splitting [9], imaging [10], chemical energy conversion and storage technologies [11], sensors and bio-sensors [4], and biomedical applications [12].

* *E-mail: abdelkhalek2@yahoo.com*

Mixed metal oxide nanocomposites (MONCs) could be defined as a multiphase solid substance possessing one, two, or three dimensions with a size less than 100 nm on the nanometer scale. The nanometric size and multifunctionality of each metal gave the nanocomposite (NC) different mechanical, electrical, optical, electrochemical, catalytic, and structural properties than those of each metal alone. The researchers concluded that the mixed MONCs stopped the bacterial cell's pathogenicity by breaking its outer and inner cell walls, which caused the cell membrane to become disorganized and leak [13]. Regarding the novel techniques for MONC formation and evaluation, several studies have been investigated [14,15]. The antibacterial capacity of co-assembled core-shelled MONCs has been characterized by the co-precipitation technique . The synthesized co-assembled MONCs of CuO, Fe_2O_3 (FeO), ZnO, ZnO/CuO–FeO_x, and ZnO–CuO–FeO showed a wide protection action against many bacterial strains [16]. Furthermore, the oxalate precursor route was recently used to synthesize CuO/c–$CuFe_2O_4$ NCs [17]. The substitution of Cu^{2+} ions by Fe^{3+} ions ($Cu_{1-X}Fe_XO$) resulted in the formation of CuO/$CuFe_2O_4$ NCs with monoclinic-like shape. The substitution within *X* values from 0 to 0.2 boosted the magnetization properties in the formed $CuFe_2O_4$ phase composite from 0.13 to 9.8 emu/g [18]. Eventually, the mechanism of MONCs depends on the generated reactive oxygen species (ROS), such as anions of superoxide radical and hydrogen peroxide, which interact with the cell wall of bacteria, leading to notable damage in the cell membrane and subsequently growth inhibition and death [19].

Several conventional antimicrobial agents that are commonly used in agriculture applications have various pros and cons [20]. Among the worldwide traditional antimicrobial products were copper(II) formate and gentamicin [21]. A copper ester of formic acid has been proven to work better against microbes when combined with other copper complexes [22,23]. Copper(II) formate has been commonly used as an antibacterial agent for coatings [24], cotton cellulose fabric curing [22], and medicinal applications [25]. Furthermore, it has been known for its antifungal activity against *Rhizoctonia solani* [26] and *Botrytis cinerea* [27]. Gentamicin, an additional aminoglycoside antibiotic used in plant agriculture, differs from streptomycin in terms of the arrangement of the heterocyclic ring and the hydroxyl substitutions linked to the amino sugars [28]. Gentamicin is considered a conventional bacteriostatic broad-spectrum antibiotic that targets the protein synthesis of the bacterial pathogen. However, it is still widely used in agriculture in developing countries as it gained approval for treating blight in apples and pears as well as certain vegetable diseases, primarily in regions of South and Central America, alongside Mexico [29].

Therefore, it is crucial to create a composite material that possesses distinct attributes to meet these requirements, such as a straightforward manufacturing process, an environmentally benign composition, long-lasting durability, and potent antimicrobial properties. In this regard, the present study focuses on the hydrothermal process of synthesizing a copper oxide–ferric oxide nanocomposite (CuO/Fe_2O_3-NC). This NC's characteristics were assessed by powder X-ray diffraction (XRD). Chemical bond formation, vibration mode analysis, and functional group identification were also identified using a Fourier transform infrared spectrophotometer. The morphological structures and elemental analysis were carried out by transmission electron microscopy (TEM). The CuO/Fe_2O_3-NC was tested for antimicrobial activity against various strains of phytopathogenic microorganisms, including fungal and bacterial isolates.

2. Materials and methods

2.1 Preparation of nanomaterials

Iron metal powder (>99%), copper nitrate ($Cu(NO_3)_2$ [>99%]), and sodium hydroxide (NaOH [>99%]) were acquired from Belaqmi Fine Chemicals, India. Bi-distilled water was used throughout the experiments. In summary, a 0.1 M solution of $Cu(NO_3)_2$ was initially prepared, followed by the addition of 4 g of iron metal powder and 10 g of NaOH. The mixture was agitated for 10 min at ambient temperature. A Teflon-coated steel autoclave was used to confine and mature the mixture for 24 h at 120°C. Subsequently, the acquired materials underwent multiple rinses with distilled water and were subsequently dried at a temperature of 60°C overnight.

2.2 Nanomaterial characterization

The crystallographic phase of the samples and their crystal size were studied by XRD with Cu-Kα radiation (Shimadzu 7000, USA). Various vibration modes, formations, chemical bonds, and function groups were determined by Fourier-transform infrared spectroscopy (FTIR), with infra-red spectra collected from 400 to 4,000 cm^{-1} (Shimadzu FTIR-8400s, Japan). This is used to identify the presence of functional groups in the obtained nanoparticles. The morphological structures and elemental analysis of the resulting nanoparticles were examined by transmittance electron microscopy (TEM; JEOL, JEM2100 plus, Japan).

2.3 Source, morphological, and molecular recognitions of fungal isolates

The fungal strains were isolated from infected strawberry plants, and the fruits showed signs of rot and gray mold. The morphological recognition of the fungal strains was performed using the identification manual illustrated by Campbell et al. [30]. The genus of fungal isolates was identified using a light microscope [31]. Amplification of the "Internal Transcribed Spacer" (ITS) area of the ribosome-encoding genes was used for the molecular identification of the fungal isolates by universal primers for ITS1 and ITS4 [32]. The polymerase chain reaction (PCR) was conducted as previously reported [33]. The final PCR products were refined and subjected to a Sanger sequencing machine. The fungal isolates were BLAST reconnoitered, and their identified sequences were coded by accession numbers using the NCBI database's GenBank portal.

2.4 Origin of bacterial isolates

The tested bacterial strains of *Pectobacterium carotovorum* (OQ878656), *Streptomyces scabies* (OR437480), *Pectobacterium atrosepticum* (MG706146), and *Ralstonia solanacearum* (OQ878653) were previously isolated from potato [34,35].

2.5 Antimicrobial activity evaluation

2.5.1 Antifungal activity

The effectiveness of CuO/Fe_2O_3-NCs in inhibiting the growth of fungal isolates was assessed using food-poisoned procedures [36]. Four concentrations of CuO/Fe_2O_3-NCs at 25, 50, 75, and 100 µg/mL were assessed utilizing potato dextrose agar (PDA) medium plates. CuO/Fe_2O_3-NCs were evaluated compared to the negative control (no chemical treatment-PDA) and the positive control (100 µg/mL copper formate-PDA). Circular paper discs (10 mm in diameter) of the tested fungal strain were laid on the PDA plates and incubated at 25°C for 7 days. The experiment was done in triplicate. The differences in radial growth diameters were expressed as inhibition percentages [37], as follows:

$$\text{Growth inhibition } \% = [(P - D)/P] \times 100,$$

where P is the mycelial growth length (mm) in the negative control (no chemical treatment-PDA), and D is the mycelial growth length (mm) of the tested CuO/Fe_2O_3-NCs-PDA.

2.5.2 Antibacterial activity

Following the agar disc-diffusion method described by Heatley [38] and modified by Balouiri et al. [39], routine antibacterial susceptibility tests were done on the chosen bacterial isolates using a final inoculum of 2×10^8 CFU/mL on agar plates with nutrient agar (NA) as the growth medium. Thereafter, filter paper discs (about 6 mm in diameter) containing CuO/Fe_2O_3-NCs at concentrations of 10, 20, 30, 40, and 50 µg/mL were placed on the agar surface compared to the negative control (no chemical treatment-NA) and the positive control (30 µg gentamicin-NA). The Petri dishes are incubated under suitable conditions of 29 ± 1°C for 2 days. The experiment was replicated three times. Finally, the antimicrobial agent diffuses into the agar and inhibits the germination and growth of the test bacterial isolates. Then, the diameters of inhibition growth zones are measured.

2.6 Data analysis

All the data obtained from the laboratory trials were analyzed using a one-way ANOVA. Significant differences in mean values were determined using the least significant difference test at a 0.05 significance level, utilizing the Statistical Analysis System (SAS) software [40].

3. Results and discussion

3.1 XRD analysis

Figure 1 displays the XRD pattern of the prepared quantum dot-composite (CuO/Fe_2O_3). The XRD peaks of the CuO nanoparticles appeared at 35.61°, 38.69°, 57.17°, 60.74°, 66.35°, and 68.45°, which correspond to (−111), (004), (200), (105), (220), and (215), respectively. This demonstrates the formation of a monoclinic (CuO) crystal structure that matches the monoclinic structure (JCPDS No. 01-076-7800) forms, as shown in Figure 1. The XRD peaks of the Fe_2O_3 nanoparticles appeared at 35.6°, 47.39°, 57.24°, and 62.86°, which correspond to (110), (207), (201), and (300), respectively (Figure 1). This shows that the Fe_2O_3 structure is hexagonal. This finding is consistent with the standard (JCPD 01-078-6916) data. The peaks then become sharper with the formation of NC (CuO/Fe_2O_3), as shown in Figure 1. The XRD patterns obtained in the sample CuO/Fe_2O_3 display the usual peaks of (−111) and (004) reflections of CuO, which are found at two values of 35.69° and 37.73°, respectively. In addition, the

XRD pattern of (110) Fe_2O_3 is found at 35.69° with a broadening shape in sample CuO/Fe_2O_3. Figure 1 shows a mix of two XRD pattern peaks (105), (220), CuO, and (201) Fe_2O_3 that appear in the range 55°–60°. This shows that the NC of CuO/Fe_2O_3 is formed. Table 1 summarizes the crystal sizes of the resulting nanoparticles. Each side of the polygon MNP had a length of approximately 12 nm. The diameter of the spherical CuO particles ranged from around 7–10 nm. Using the Debye–Scherer equation [41], the crystal diameters of all the nanoparticles obtained can be determined as follows:

$$D = \frac{K\lambda}{\beta \cos \theta},$$

where λ is the Cu-Kα wavelength (0.1542 nm), β is the FWHM, and K is a constant.

Peak	2θ	Plane	FWHM	Size (nm)
1	35.61	−111 (CuO)	1.235	7
2	43.37	400 (CuO/Fe_2O_3)	0.7399	12
3	44.73	−112 (CuO)	0.842	10.6
4	31.25	110 (CuO)	0.963	9

Table 1. Calculated crystal sizes of the obtained quantum dot.

3.2 FTIR results

The produced NC was analyzed using FTIR spectroscopy to determine the functional groups present [42]. Figure 2 shows the FTIR spectrum of CuO/Fe_2O_3. It has noticeable characteristic peaks at 525 cm^{-1} which belong to the bending vibration of the Cu–O bond [43]. The strong band below 700 cm^{-1} reveals the Fe–O stretching mode. The band corresponding to the Fe–O stretching mode of Fe_2O_3 is shown at 567 cm^{-1} [44]. Briefly, all prepared metal oxide nanomaterials were characterized by bending vibration of the metal–O bond, CuO, and Fe_2O_3, which appeared in a broad band at around ν 500 cm^{-1} [45]. The FTIR results are consistent with the XRD patterns of the NC (CuO/Fe_2O_3) and confirm the chemical reaction that takes place during the hydrothermal treatment of copper hydroxide and iron(III) oxide-hydroxide, leading to the creation of the NC (CuO/Fe_2O_3).

3.3 Chemical reaction

$$\text{Fe(metal)} + 2\text{NaOH} + \text{Cu(NO}_3\text{)}_2 \rightarrow \text{Cu(OH)}_2 + \text{Fe(OH)}_3 + 2\text{NaNO}_3, \quad (2)$$

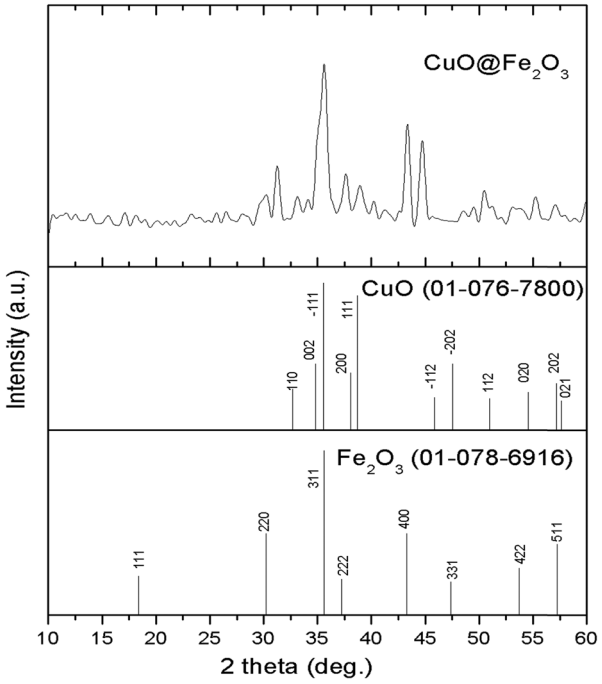

Figure 1. XRD pattern of the prepared nanoparticles; CuO, Fe_2O_3, and the NC CuO/Fe_2O_3.

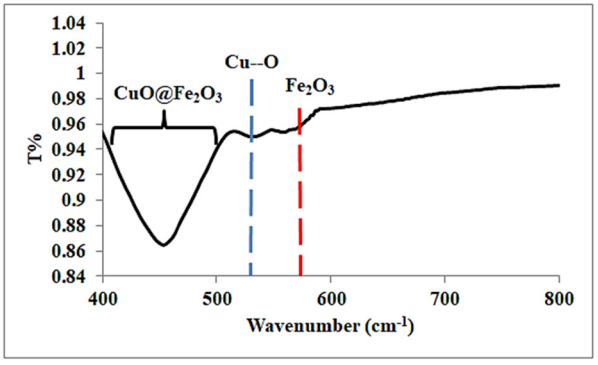

Figure 2. FTIR spectrum of the prepared NC (CuO/Fe_2O_3).

$$Cu(OH)_2 + 2Fe(OH)_3 \rightarrow (\text{Hydrothermal treatment}) \rightarrow CuO + Fe_2O_3 + 4H_2O. \quad (3)$$

The elemental analyses of the prepared nanomaterials were determined by energy-dispersive X-ray spectroscopy (EDX). We detected the percentage and type of each element present. Figure 3 displays the EDX of the prepared NC (CuO/Fe_2O_3), as well as the percentage and type of each containing element. EDX confirms the presence of Cu, Fe, and O with weight percent. The EDX results then align with the XRD and FTIR results. As shown in the EDX results, the current percentage of iron is nearly double the copper element percentage. Figure 4 shows the TEM micrograph of the obtained NC (CuO/Fe_2O_3). It is noticeable that it contains two mixed shapes: the polygon shape of the NC, which consists of a spherical shape of CuO, and plate-like-shaped Fe_2O_3 quantum dots. These findings are consistent with the results reported in a previous publication [4].

3.4 Identification and growth response of fungal isolates to CuO/Fe_2O_3-NC

The isolated fungi were identified as *Fusarium oxysporum*, *B. cinerea*, and *R. solani* through morphological and molecular analysis. These fungi may be found in GenBank with the accession codes OR116510, OR116494, and OR116531, respectively. The results presented in Table 2 demonstrate the growth response of the chosen fungal isolates to the CuO/Fe_2O_3 NC at various concentrations (25, 50, 75, and 100 µg/mL). The growth response was compared to both

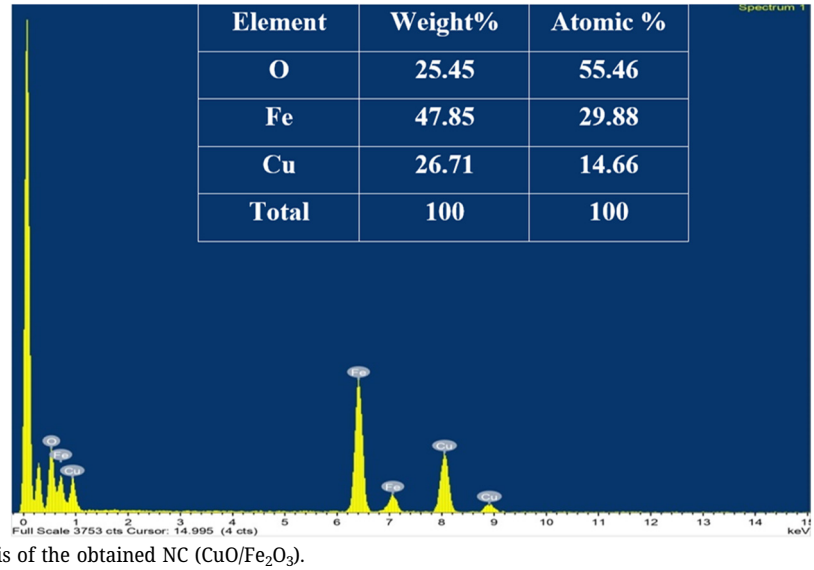

Figure 3. EDX analysis of the obtained NC (CuO/Fe_2O_3).

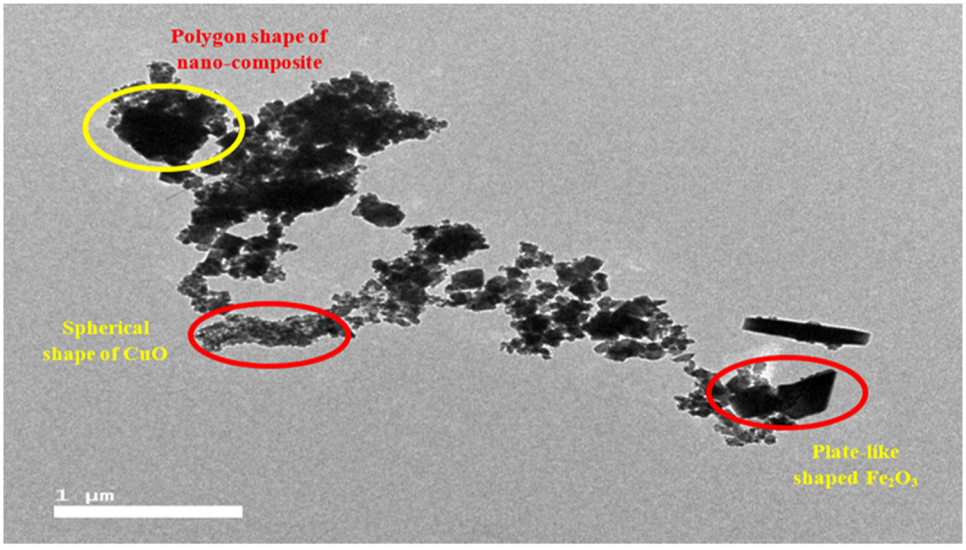

Figure 4. TEM micrograph of the obtained NC (CuO/Fe_2O_3).

negative controls (without chemical treatment) and positive controls (copper formate at a concentration of 100 µg/mL).

The growth of the fungal isolates that were tested was significantly slowed down by CuO/Fe_2O_3 NCs and copper formate at different concentrations when compared to the negative control. The smallest growth diameters for *F. oxysporum* were found in CuO/Fe_2O_3-NCs, which are similar to copper formate. These were 26.3 and 26 mm at 75 and 100 µg/mL, respectively. In the same way, the smallest *B. cinerea* growth measurements were 50, 46.3, and 45 mm when CuO/Fe_2O_3-NCs were used at 50, 75, and 100 µg/mL, respectively. In contrast, copper formate effectively counteracted the inhibitory impact of all concentrations of CuO/Fe_2O_3 NC on *R. solani*. According to the results shown above, CuO/Fe_2O_3-NCs at a concentration of 100 µg/mL had the best effect on stopping *B. cinerea*, with a 50% success rate. Copper formate at a concentration of 100 µg/mL had the best inhibition percentages against *F. oxysporum* (71.5%) and *R. solani* (82.2%). Eltarahony et al. [46] verified these results and found that metal oxide hybrid NCs possess remarkable capability to penetrate and disrupt the inflexible composition of glycoprotein–glucan–chitin in the fungal cell wall. In this case, a biogenic Cu/Fe hybrid NC exhibited significant protection against the fungus *Candida albicans* at concentrations of 250 and 500 µg/mL. Parameswaran et al. [47] evaluated the antifungal properties of the Co/CeO_2 NCs against *C. albicans* and *Aspergillus fumigatus*. The findings indicated that Co/CeO_2 NCs serve as a moderate antifungal agent for both *C. albicans* and *A. fumigatus*. At a concentration of 30 µL, the inhibition zones measured 12 mm for

Concentrations (µg/mL)	Growth response (diameter [mm] ± SD[1]; inhibition [%])					
	Fusarium oxysporum		*Botrytis cinerea*		*Rhizoctonia solani*	
	(OR116510)		(OR116494)		(OR116531)	
25	29.3 ± 0.58^{b}	67.4	53.7 ± 4.04^{b}	40.4	19.7 ± 0.58^{b}	78.2
50	28.0 ± 1.73^{b,c}	68.9	50.0 ± 0.00^{b,c}	44.4	18.0 ± 0.00^{c}	80.0
75	26.3 ± 1.53^{c,d}	70.7	46.3 ± 1.15^{c,d}	48.5	18.0 ± 0.00^{c}	80.0
100	26.0 ± 0.00^{d}	71.1	45.0 ± 3.00^{d}	50.0	17.0 ± 0.00^{d}	81.1
−ve control[2]	90.0 ± 0.00^{a}	0.00	90.0 ± 0.00^{a}	0.00	90.0 ± 0.00^{a}	0.00
+ ve control[3]	25.7 ± 1.15^{d}	71.5	46.7 ± 0.58 cd	48.5	16.0 ± 1.00^{e}	82.2

Similarity in the letters adjacent to the growth values in each column is not significantly distinguished as per the $LSD_{0.05}$.
[1] Standard deviation. [2] Without CuO/Fe_2O_3-NC treatment. [3] Copper formate (100 µg/mL).

Table 2. Hyphal growth response of the fungal isolates to series concentrations of CuO/Fe_2O_3-NCcompared to copper formate after 7 days of incubation.

C. albicans and 14 mm for *A. fumigatus*, compared to 22 mm for the standard antifungal agents. As an antifungal agent, the copper formate complex exhibited a significant inhibitory effect on the growth of *R. solani* at a concentration of 200 µg/mL [26], as well as effectively reducing the infection of *Rosa hybrida* flowers by *B. cinerea* at a concentration of 1,000 mg/L [27]. In a recent study [48], an innovative NC was synthesized using mycosynthesized bimetallic zinc–copper oxide nanoparticles, nanocellulose, and chitosan, and the results demonstrated significant antifungal activity against *Aspergillus brasiliensis* with an MIC of 7.81 µg/mL. However, the NC had limited antifungal effectiveness against *Cryptococcus neoformans* and *C. albicans*, with an MIC of 250 µg/mL for both. However, it was evident that smaller particles enhance the interaction between nanoparticles and fungal cells, allowing them to penetrate bacterial and fungal cell walls more easily [49].

3.5 Inhibition zone of bacterial isolates to CuO/Fe_2O_3-NC

The findings indicated that the synthesized CuO/Fe_2O_3-NCs effectively suppressed the growth of bacterial isolates at doses of 10, 20, 30, 40, 50, and 100 µg/mL, as compared to the negative control (no chemical treatment) and positive control (gentamicin, 30 µg) (Table 3). It was noted that gentamicin exhibited the most potent inhibition zones against the selected bacterial isolates, surpassing the inhibitory effects of all tested doses of CuO/Fe_2O_3-NCs. Furthermore, all of the tested concentrations exhibited inhibition zones compared to the negative control (Table 3). All the assigned concentrations of CuO/Fe_2O_3-NCs showed equipollent inhibitions on *P. carotovorum* and *S. scabies.* At the same time, 40 and 50 µg/mL of CuO@ Fe_2O_3 NCs were the most effective amounts against *P. atrosepticum*, with inhibition zones measuring 9.33 and 10.67 mm. Similarly, CuO/Fe_2O_3-NCs at 50 µg/mL achieved the highest inhibition zone of 14.7 mm against *R. solanacearum.*

The data can be interpreted by considering the mechanism of MONCs, which involves the generation of ROS, such as superoxide radicals and hydrogen peroxide anions. These ROS can attack bacteria's cell walls, causing damage to the membrane and internal organelles, ultimately leading to growth inhibition or even cell death [19]. Moreover, it was concluded that the MONCs, $Fe_2O_3@Cu_2O$, showed inhibitory effects on the pathogenicity of the bacterial cell by rupturing its outer and inner cell walls to cause disorganization and leakage in the cell membrane [13]. In addition, the co-assembled core-shelled MONCs, $ZnO–Fe_2O_{3x}–CuO_x$ using the co-precipitation technique, demonstrated obvious anti-growth activity against bacterial cells. For instance, the anti-growth activity was clearly exhibited in the descending order for the co-assembled core-shelled MONCs of CuO > $ZnOFeO_{0.5}CuO_{0.5}$ > $CuOFeO_{0.5}$ > $ZnOFeO_{0.1}CuO_{0.1}$ > Fe_2O_3 > $ZnOFeO_{0.5}$ > ZnO against *Staphylococcus pneumonia* [16]. Conversely, copper formate and copper formate-based NPs possessed an antimicrobial augmentation synergized with Cu(II) ions, having the ability to generate free radicals that could promote disordering in the cell membrane and lipid peroxidation within the bacteria. In particular, the cell membranes of *Staphylococcus aureus* and *Escherichia coli* were robust and unruffled in the control-treated groups compared to the copper formate-treated groups, which had some puckers on the cell membranes leading to the release of cytoplasm from the bacterial cells [25]. The antibacterial properties of Co/CeO_2 NCs were tested against four pathogenic bacteria: *E. coli*, *S. aureus*, *Salmonella paratyphi*, and *Klebsiella pneumonia* at a concentration of 30 µL. The results indicate that CeO_2 inhibited the growth of all bacteria. Specifically, *K. pneumonia* showed an inhibition zone of 18 mm, while *E. coli*, *S. aureus*, and *S. paratyphi* exhibited inhibition zones

Concentrations (µg/mL)	Inhibition zone (diameter [mm] ± SD[1])			
	P. carotovorum	*S. scabies*	*P. atrosepticum*	*R. solanacearum*
10	11.0 ± 0.00^{b}	9.00 ± 0.00^{b}	9.00 ± 0.00^{c}	10.7 ± 0.58^{d}
20	11.0 ± 0.00^{b}	9.00 ± 0.00^{b}	9.00 ± 0.00^{c}	11.0 ± 0.00^{d}
30	11.7 ± 0.58^{b}	9.00 ± 0.00^{b}	9.00 ± 0.00^{c}	11.0 ± 0.00^{d}
40	11.7 ± 0.58^{b}	9.00 ± 0.00^{b}	9.33 ± 0.58^{c}	12.0 ± 0.00^{c}
50	12.3 ± 1.15^{b}	9.00 ± 0.00^{b}	10.7 ± 0.58^{b}	14.7 ± 0.58^{b}
−ve control[2]	0.00 ± 0.00^{c}	0.00 ± 0.00^{c}	0.00 ± 0.00^{d}	0.00 ± 0.00^{e}
+ ve control[3]	19.0 ± 1.73^{a}	41.7 ± 2.89^{a}	16.00 ± 1.73^{a}	25.0 ± 0.00^{a}

Similarity in the letters adjacent to the growth values in each column is not significantly distinguished as per the $LSD_{0.05}$.
[1] Standard deviation. [2] Without CuO/Fe_2O_3-NC treatment. [3] Gentamicin (30 µg/disc).
Table 3. Inhibition zone of the bacterial isolates to series concentrations of CuO/Fe_2O_3-NC compared to gentamicin.

of 12, 14, and 16 mm, respectively. In comparison, amoxicillin (10 µL) created inhibition zones of 22 mm against *E. coli*, *S. aureus*, and *S. paratyphi*, and 24 mm against *K. pneumonia*, indicating slightly higher effectiveness than Co/CeO_2 NCs [47]. To prepare antimicrobial composites, different methods were used, including physically combining methylphenyl silicone resin with two plants, *Houttuynia* and *Scutellarin*, to create antifouling coatings. The prepared coatings exhibited inhibition rates of 90% against *S. aureus* and *E. coli* [50].

The antibacterial mechanisms of NCs are varied, often involving smaller particles that possess larger surface areas and can penetrate cells more easily, leading to cell death. The interaction between NCs and bacterial cell walls, due to electrostatic attraction, also contributes to bacterial cell death [51]. Ansari et al. [52] demonstrated the antibacterial activity of TiO_2 against *Pseudomonas aeruginosa* and *S. aureus* at a concentration of 2 mg/mL. Similarly, Almessiere et al. [51] reported the antibacterial effects of Ce^{3+}/Dy^{3+} co-activated Mn–Zn nanospinel ferrites against *E. coli* and *S. aureus*. However, the inhibition effects of both pure CeO_2 and Co/CeO_2 NCs were not as pronounced as those of the antibiotics used as positive controls. Zhang et al. [53] analyzed ternary lanthanide coordination polymers (LCPs) against several bacterial strains, revealing MIC and MBC values ranging from 50 to 400 ppm. 8-Hydroxyquinoline showed the most potent antibacterial action, while other composites had comparable MIC and MBC values. The MIC/MBC values showed greater efficacy against Gram-positive bacteria like *S. aureus*. TEM analysis showed a bactericidal process in *E. coli*, confirming LCPs' ability to kill bacteria.

The antimicrobial activities of NPs were subjectively determined by their characteristics, such as size, shape, concentration, and physicochemical properties [54]. The current results confirm that the obtained CuO/Fe_2O_3-NC has remarkable antimicrobial capabilities.

4. Conclusions

In conclusion, the hydrothermal process for synthesizing CuO/Fe_2O_3 NCs provides a flexible approach that has a wide range of antibacterial capabilities. The CuO/Fe_2O_3 NCs were analyzed using XRD, FTIR, and TEM techniques and were tested against specific fungal and bacterial isolates. The inhibitory effects of CuO/Fe_2O_3-NCs on *F. oxysporum* and *B. cinerea* were shown to be similar to those of copper formate. Nevertheless, controls containing copper exhibited superior performance compared to CuO/Fe_2O_3-NCs when tested against *R. solani* and all bacterial strains. However, CuO/Fe_2O_3-NCs exhibited notable inhibitory effects on *P. carotovorum*, *S. scabies*, *P. atrosepticum*, and *R. solanacearum*, indicating their potential as strong antibacterial agents against these specific diseases. Therefore, incorporating further modifications and improvements in the methods employed for preparation could lead to a wide range of antimicrobial effects.

Acknowledgments

The authors would like to extend their appreciation to the Researchers Supporting Project number (RSP2024R505), King Saud University, Riyadh, Saudi Arabia.

Author contributions

Conceptualization and methodology: M.E., M.N., S.B., A.A. Software and validation: M.N., M.E., A.A. Formal analysis and writing – original draft: M.N., M.E., S.B., A.A.Al., P.K., and A.A. Supervision: A.A. All co-authors reviewed the final version and approved the manuscript before submission.

Conflict of interest statement

The authors declare no conflict of interest.

Data availability statement

The datasets used and/or analyzed through this study are accessible from the corresponding author upon reasonable request.

References

[1] Abdelmoneim, H.M., Taha, T.H., Elnouby, M.S., AbuShady, H.M., Extracellular biosynthesis, OVAT/statistical optimization, and characterization of silver nanoparticles (AgNPs) using leclercia adecarboxylata THHM and its antimicrobial activity, Microb. Cell Fact., 2022, 21: 277

[2] Ali, A., Zafar, H., Zia, M., ul Haq, I., Phull, A.R., Ali, J.S., et al., Synthesis, characterization, applications, and challenges of iron oxide nanoparticles, Nanotechnol. Sci. Appl., 2016, 9: 49–67

[3] Samrot, A.V., Sahithya, C.S., Selvarani, J., Purayil, S.K., Ponnaiah, P., A review on synthesis, characterization

and potential biological applications of superparamagnetic iron oxide nanoparticles, Curr. Res. Green. Sustain. Chem., 2021, 4: 100042
[4] Elnouby, M.S., Taha, T.H., Abu-Saied, M.A., Alamri, S.A., Mostafa, Y.S.M., Hashem, M., Green and chemically synthesized magnetic iron oxide nanoparticles-based chitosan composites: preparation, characterization, and future perspectives, J. Mater. Sci. Mater Electron., 2021, 32: 10587–10599
[5] Moustafa, M., Alamri, S., Elnouby, M., Taha, T., Abu-Saied, M.A., Shati, A., et al., Hydrothermal preparation of TiO_2-Ag nanoparticles and its antimicrobial performance against human pathogenic microbial cells in water, Biocell, 2018, 42: 93
[6] Aragaw, T.A., Bogale, F.M., Aragaw, B.A., Iron-based nanoparticles in wastewater treatment: a review on synthesis methods, applications, and removal mechanisms, J. Saudi Chem. Soc., 2021, 25: 101280
[7] Montiel Schneider, M.G., Martín, M.J., Otarola, J., Vakarelska, E., Simeonov, V., Lassalle, V., et al., Biomedical applications of iron oxide nanoparticles: current insights progress and perspectives, Pharmaceutics, 2022, 14: 204
[8] Zhao, H., Zhu, Q., Gao, Y., Zhai, P., Ma, D., Iron oxide nanoparticles supported on pyrolytic graphene oxide as model catalysts for Fischer Tropsch synthesis, Appl. Catal. A Gen., 2013, 456: 233–239
[9] Tartaj, P., Morales, M.P., Gonzalez-Carreño, T., Veintemillas-Verdaguer, S., Serna, C.J., The iron oxides strike back: From biomedical applications to energy storage devices and photoelectrochemical water splitting, Adv. Mater., 2011, 23: 5243–5249, doi: 10.1002/adma.201101368
[10] Baig, N., Kammakakam, I., Falath, W., Nanomaterials: a review of synthesis methods, properties, recent progress, and challenges, Mater. Adv., 2021, 2: 1821–1871
[11] Khan, I., Saeed, K., Khan, I., Nanoparticles: properties, applications and toxicities, Arab. J. Chem., 2019, 12: 908–931
[12] Tran, H.-V., Ngo, N.M., Medhi, R., Srinoi, P., Liu, T., Rittikulsittichai, S., et al., Multifunctional iron oxide magnetic nanoparticles for biomedical applications: a review, Materials (Basel), 2022, 15: 503
[13] Birhanu, R., Afrasa, M.A., Hone, F.G., Recent progress of advanced metal-oxide nanocomposites for effective and low-cost antimicrobial activates: a review, J. Nanomater., 2023, 2023: 1–25
[14] Jin, P., Dalgarno, S.J., Atwood, J.L., Mixed metal-organic nanocapsules, Coord. Chem. Rev., 2010, 254: 1760–1768
[15] Su, Y., Shen, Z., Long, X., Chen, C., Qi, L., Chao, X., Gaussian filtering method of evaluating the elastic/elasto-plastic properties of sintered nanocomposites with quasi-continuous volume distribution, Mater. Sci. Eng. A, 2023, 872: 145001
[16] Owonubi, S.J., Ateba, C.N., Revaprasadu, N., Co-assembled ZnO-Fe_2O_{3x}-CuO_x nano-oxide materials for antibacterial protection, Phosphorus Sulfur Silicon Relat. Elem., 2020, 195: 981–987
[17] Eldesouky, S.E., Aseel, D.G., Elnouby, M.S., Galal, F.H., Al-Farga, A., Hafez, E.E., et al., Synthesis of tungsten oxide, iron oxide, and copper-doped iron oxide nanocomposites and evaluation of their mixing effects with cyromazine against *Spodoptera littoralis* (boisduval), ACS Omega, 2023, 8: 44867–44879
[18] Rashad, M.M., Rayan, D.A., Ramadan, A.A., Optical and magnetic properties of CuO/$CuFe_2O_4$ nanocomposites, J. Mater. Sci. Mater. Electron., 2013, 24: 2742–2749
[19] Pachaiappan, R., Rajendran, S., Show, P.L., Manavalan, K., Naushad, M., Metal/metal oxide nanocomposites for bactericidal effect: a review, Chemosphere, 2021, 272: 128607
[20] Attarilar, S., Yang, J., Ebrahimi, M., Wang, Q., Liu, J., Tang, Y., et al., The toxicity phenomenon and the related occurrence in metal and metal oxide nanoparticles: a brief review from the biomedical perspective, Front. Bioeng. Biotechnol., 2020, 8: 822
[21] Lu, W., Wang, M., Wu, J., Jiang, Q., Jin, J., Jin, Q., et al., Spread of chloramphenicol and tetracycline resistance genes by plasmid mobilization in agricultural soil, Environ. Pollut., 2020, 260: 113998
[22] Rose, G.R.F., Howdon, J.B., Bayley, C.H., Observations on the use of copper formate as a rotproofer for cotton fabric, Text. Res. J., 1959, 29: 996–1005, doi: 10.1177/004051755902901210
[23] Rossmoore, H.W., The interaction of formaldehyde, isothiazolone and copper, Int. Biodeterior., 1990, 26: 225–235, doi: 10.1016/0265-3036(90)90062-C
[24] Abrams, E., Bottoms, R.R., A copper process for prolonged microbiological protection of cellulosic fabrics by chemical modification, Text. Res. J., 1956, 26: 630–640, doi: 10.1177/004051755602600808
[25] Zhou, Y., Sun, P., Cao, Y., Yang, J., Wu, Q., Peng, J., Biocompatible copper formate-based nanoparticles with strong antibacterial properties for wound healing, J. Nanobiotechnol., 2023, 21: 474
[26] Aamer, H.A., Al-Askar, A.A., Gaber, M.A., El-Tanbouly, R., Abdelkhalek, A., Behiry, S., et al., Extraction, phytochemical characterization, and antifungal activity of Salvia rosmarinus extract, Open. Chem., 2023, 21: 20230124, doi: 10.1515/chem-2023-0124

[27] Hammer, P.E., Evensen, K.B., Janisiewicz, W.J., Postharvest control of botrytis cinerea infections on cut rose flowers with pyrrolnitrin, HortScience, 2019, 25: 1139a, doi: 10.21273/hortsci.25.9.1139a
[28] Miller, S.A., Ferreira, J.P., LeJeune, J.T., Antimicrobial use and resistance in plant agriculture: a one health perspective, Agriculture, 2022, 12: 289
[29] Stockwell, V.O., Duffy, B., Use of antibiotics in plant agriculture, Rev. Sci. Tech. Int. Des. Epizoot., 2012, 31: 199–210
[30] Campbell, C.K., Johnson, E.M., Warnock, D.W. Identification of pathogenic fungi, John Wiley & Sons, Hoboken, NJ, USA, 2013, doi: 10.1002/9781118520055
[31] Dugan, F.M. The identification of fungi: an illustrated introduction with keys, glossary, and guide to literaturey, APS Press, Saint Paul, MN, USA, 2006, doi: 10.1094/9780890545041
[32] White, T.J., Bruns, T., Lee, S., Taylor, J., Amplification and direct sequencing of fungal ribosomal rna genes for phylogenetics, PCR Protoc., 1990, 18: 315–322, doi: 10.1016/b978-0-12-372180-8.50042-1
[33] Soliman, S.A., Al-Askar, A.A., Sobhy, S., Samy, M.A., Hamdy, E., Sharaf, O.A., et al., Differences in pathogenesis-related protein expression and polyphenolic compound accumulation reveal insights into tomato–pythium aphanidermatum interaction, Sustainability, 2023, 15: 6551
[34] El-Bilawy, E.H., Al-Mansori, A.-N.A., Soliman, S.A., Alotibi, F.O., Al-Askar, A.A., Arishi, A.A., et al., Antifungal, antiviral, and HPLC analysis of phenolic and flavonoid compounds of amphiroa anceps extract, Sustainability, 2022, 14: 12253
[35] Al-Askar, A.A., Bashir, S., Mohamed, A.E., Sharaf, O.A., Nabil, R., Su, Y., et al., Antimicrobial efficacy and HPLC analysis of polyphenolic compounds in a whole-plant extract of *Eryngium campestre*, Separations, 2023, 10: 362
[36] Kumar, A., Shukla, R., Singh, P., Prasad, C.S., Dubey, N.K., Assessment of *Thymus vulgaris* L. essential oil as a safe botanical preservative against post harvest fungal infestation of food commodities, Innov. Food Sci. Emerg. Technol., 2008, 9: 575–580, doi: 10.1016/j.ifset.2007.12.005
[37] Hamdy, E., El-Gendi, H., Al-Askar, A., El-Far, A., Kowalczewski, P., Behiry, S., et al., Copper oxide nanoparticles-mediated Heliotropium bacciferum leaf extract: antifungal activity and molecular docking assays against strawberry pathogens, Open. Chem., 2024, 22: 20240028, doi: 10.1515/chem-2024-0028
[38] Heatley, N.G., A method for the assay of penicillin, Biochem. J., 1944, 38: 61
[39] Balouiri, M., Sadiki, M., Ibnsouda, S.K., Methods for in vitro evaluating antimicrobial activity: a review, J. Pharm. Anal., 2016, 6: 71–79, doi: 10.1016/j.jpha.2015.11.005
[40] Statistical Analysis System (SAS). Institute INC, PC-SAS user guide, version 8. North Carolina Statistical Analysis System Institute, Inc., Cary, NC 27513, USA, 2002
[41] Ramadan, M., Elnouby, M.S., El-Shazly, O., El-Wahidy, E.F., Farag, A.A.M., Roushdy, N., Facile fabrication, structural and electrical investigations of cadmium sulfide nanoparticles for fuel cell performance, Mater. Renew. Sustain. Energy, 2022, 11: 1–10
[42] Taha, T.H., Abu-Saied, M.A., Elnouby, M.S., Hashem, M., Alamri, S., Mostafa, Y., Designing of pressure-free filtration system integrating polyvinyl alcohol/chitosan-silver nanoparticle membrane for purification of microbe-containing water, Water Supply, 2019, 19: 2443–2452
[43] Nabil, M., Motaweh, H.A., Dendritic porous silicon as a heavy metal removal (copper element), Евразийский Союз Yченых, 2019, 4: 55–59
[44] Farahmandjou, M., Soflaee, F., Synthesis and characterization of α-Fe_2O_3 nanoparticles by simple co-precipitation method, Phys. Chem. Res., 2015, 3: 191–196
[45] Nabil, M., Mahmoud, K.R., Nomier, R., El-Maghraby, E.-M., Motaweh, H., Nano-porous-silicon powder as an environmental friend, Materials (Basel), 2021, 14: 4252
[46] Eltarahony, M., Abu-Serie, M., Hamad, H., Zaki, S., Abd-El-Haleem, D., Unveiling the role of novel biogenic functionalized CuFe hybrid nanocomposites in boosting anticancer, antimicrobial and biosorption activities, Sci. Rep., 2021, 11: 7790
[47] Parameswaran, S., Bakkiyaraj, R., Shanmugam, P., Boonyuen, S., Venugopal, T., Investigation of biological efficacy assessment of cobalt-doped cerium oxide nanocomposites against pathogenic bacteria, fungi, and lung cancer cells, Mater. Chem. Phys., 2024, 321: 129496
[48] Hasanin, M.S., Hashem, A.H., Al-Askar, A.A., Haponiuk, J., Saied, E., A novel nanocomposite based on mycosynthesized bimetallic zinc-copperoxide nanoparticles, nanocellulose and chitosan: characterization, antimicrobial and photocatalytic activities, Electron. J. Biotechnol., 2023, 65: 45–55
[49] Raghupathi, K.R., Koodali, R.T., Manna, A.C., Size-dependent bacterial growth inhibition and mechanism of antibacterial activity of zinc oxide nanoparticles, Langmuir, 2011, 27: 4020–4028

[50] He, G., Li, H., Zhao, Z., Liu, Q., Yu, J., Ji, Z., et al., Antifouling coatings based on the synergistic action of biogenic antimicrobial agents and low surface energy silicone resins and their application to marine aquaculture nets, Prog. Org. Coat., 2024, 195: 108656
[51] Almessiere, M.A., Slimani, Y., Rehman, S., Khan, F.A., Güngüneş, ÇD, Güner, S., et al., Magnetic properties, anticancer and antibacterial effectiveness of sonochemically produced Ce^{3+}/Dy^{3+} co-activated Mn-Zn nanospinel ferrites, Arab. J. Chem., 2020, 13: 7403–7417
[52] Ansari, M.A., Albetran, H.M., Alheshibri, M.H., Timoumi, A., Algarou, N.A., Akhtar, S., et al., Synthesis of electrospun TiO_2 nanofibers and characterization of their antibacterial and antibiofilm potential against gram-positive and gram-negative bacteria, Antibiotics, 2020, 9: 572
[53] Zhang, L., Shi, H., Tan, X., Jiang, Z., Wang, P., Qin, J., Ten-gram-scale mechanochemical synthesis of ternary lanthanum coordination polymers for antibacterial and antitumor activities, Front. Chem., 2022, 10: 898324
[54] El-Moslamy, S.H., Elnouby, M.S., Rezk, A.H., El-Fakharany, E.M., Scaling-up strategies for controllable biosynthetic ZnO NPs using cell free-extract of endophytic *Streptomyces albus*: characterization, statistical optimization, and biomedical activities evaluation, Sci. Rep., 2023, 13: 3200